Computers & Graphics (2018)

Contents lists available at ScienceDirect

Computers & Graphics

journal homepage: www.elsevier.com/locate/cag

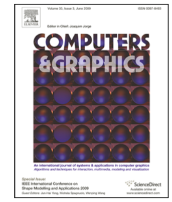

Design and Analysis of Directional Front Projection Screens

Michal Piovarči[a,b], Michael Wessely[a,c], Michał Jagielski[a], Marc Alexa[d], Wojciech Matusik[e], Piotr Didyk[a,b,f]

[a] *Saarland University, MMCI*
[b] *MPI Informatik*
[c] *Inria, Univ. Paris-Sud, CNRS, Université Paris-Saclay*
[d] *TU Berlin*
[e] *MIT CSAIL*
[f] *Università della Svizzera italiana*

ARTICLE INFO

Article history:
Received August 8, 2018

Keywords: Computational Fabrication, Reflectance, Energy Efficiencent Screens

ABSTRACT

Traditional display and screen are designed to maximize the perceived image quality across all viewing directions. However, there is usually a wide range of directions (e.g., towards side walls and ceiling) for which the displayed content does not need to be provided. Ignoring this fact results in energy waste due to a significant amount of light reflected towards these regions. In this work, we propose a new type of front projection screens – *directional screens*. They are composed of tiny, highly reflective surfaces which reflect the light coming from a projector only towards the audience. Additionally, they avoid "hot-spotting" and can support non-standard audience layouts. In this paper, we describe the design process as well as provide feasibility analysis of the new screens. We also validate the approach in simulations and by fabricating several fragments of big screens. We demonstrate that thanks to the customization, our solution can provide up to three times increased gain when compared to traditional high gain screens and up to eight times higher brightness than a matte screen.

© 2018 Elsevier B.V. All rights reserved.

1. Introduction

Continuous demand for higher quality image reproduction forces displays manufacturers to refine their designs constantly. While many hardware and software solutions for improving display quality exist, the efficient use of emitted light is often overlooked, and the increase in display quality comes at the price of energy efficiency. For instance, a display system usually provides high-quality brightness and color reproduction independently of the viewer position, which is often unnecessary and becomes evident in the movie theater scenario, where the audience layout is precisely defined. In such cases, it is sufficient to provide high image quality only for positions where the audience is expected and avoid emitting light in other directions, e.g., the walls or ceiling.

Efficient use of light can also lead to brighter screens. This becomes very important for 3D movie theaters, where the overall brightness is reduced to roughly 20% of its initial value [1]. Given that the standard brightness for 2D cinema is 14-16 fL (footlambert) (48-55 cd/m^2), using the same projector for 3D applications results in around 3 fL (10 cd/m^2). This has significant implications for perceived quality. In such conditions, human perception operates on the boundary between mesopic and photopic vision, where spatial acuity, perceived contrast, depth perception, and color vision are significantly affected [2, 3, 4]. A natural solution to the problem is to provide brighter projectors [5]. This, however, leads to significantly increased operating costs since brighter projection lamps consume more energy are more expensive and burn out more quickly. As a consequence, brightening a projector can potentially quadruple the annual maintenance cost [6]. More efficient solutions are projectors that use additional optical components, such as digital micromirror devices or phase modulators, to redistribute the light according to the required brightness [7, 8]. Comple-

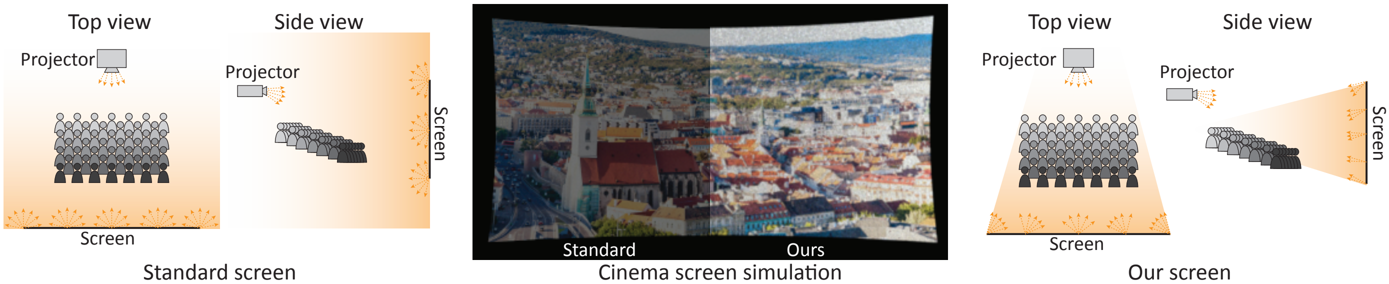

Fig. 1. Current screens reflect a lot of light into regions where the audience is not expected (left). Reflecting the light toward the ceiling, floor or walls is unnecessary and causes energy loss. Our design enables fine control over the reflectance properties of the screen surface (right), which provides better energy efficiency, brightness, and contrast.

mentary efforts focus on designing a light-efficient screen. In this context, the common strategy is to use high-gain screens which boost the brightness but suffer from hot-spotting, i.e., a brightness fall-off towards the boundaries, due to their significant specular component.

In this work, we propose a new technique for designing large light-efficient front projection cinema screens [9]. Similarly to [10, 11, 12] we took a geometrical approach to the design of cinema screens. We treat a cinema screen as a large area with a prescribed spatially-varying reflectance that reflects the light only towards the audience (Figure 1). To build such a screen, we use small geometric components. Each component is built from micro-mirrors with carefully designed normals that reflect the light only in precisely defined range. We formulate the search for such geometries as a convex optimization that guarantees correct normal distribution and tileability of our shapes. As our screens are made of a highly reflective surface, they preserve polarization, and therefore they can be used in 3D movie theaters. We evaluated our technique using simulations, as well as capturing several manufactured screen parts. Besides designing standard screens, e.g., for movie theaters, our technique can be used in more challenging cases. We demonstrate this by producing a screen which reflects the light into two disjoint regions. This paper is an extended version of [9]. Besides the description of the method and initial results presented previously, we provide a detailed analysis of screen layouts that can be generated using our method and define theoretical and practical limitations of directional screens. Additionally, we include an extended discussion and evaluation of image brightness and quality.

2. Previous Work

To maximize light efficiency, an optimal screen should reflect light only towards the audience. As the required angular light coverage varies across the screen (Figure 1), the optimal solution requires producing a surface with spatially-varying reflectance properties (SVBRDF). This problem is not only relevant for screen design, but it has also been broadly researched in the context of appearance reproduction. In this section, we will discuss the work from both fields. Our technique is also related to reflector designs, where the shape of a highly reflective surface is optimized to reflect light in the desired direction. We refer the reader to the following survey for discussion of these techniques [13].

Screen Design. Over last several decades, screen design evolved from a simple, Lambertian-like surface (i.e., a matte screen), which reflects light uniformly in all directions, to more sophisticated ones, where both the material as well as the geometrical structure of the screen are carefully designed to maximize the portion of light reflected towards the audience. The simplest solutions involve covering the screen surface with a semi-glossy coating [14]. Such screens are usually characterized by their gain factor, which is a ratio of the light reflected by the screen as compared to the light reflected from a matte screen. Although they provide better efficiency, they suffer from a “hot-spot” effect, i.e., the observed brightness is uniform neither across the screen nor at different viewing locations. Additionally, the highest gain is achieved only for a center position in the audience [15]. The problem can be reduced to a certain extent by using a curved screen geometry [16]. Finer control over the screen reflectance properties can be achieved by modifying the local geometry of a highly reflective surface. Although several commercial solutions have been proposed [17, 18, 19, 20], it is unclear how optimal these solutions are, as there is not enough detail to faithfully reproduce or simulate the designs, and no qualitative evaluation is provided.

One of the most recent solutions in this area was proposed by Coleman et al. [21]. Similarly to us, they take a purely geometrical approach, i.e., they build the screen using a mirror-like surface and control the reflectance properties by careful design of the screen surface. They proposed to construct the surface out of small kernel-like shapes designed according to the desired reflectance. They show how to tile such shapes to obtain the entire screen surface. Although they can vary the shapes locally, their method assumes that the shapes are axially symmetric. This limits their flexibility in adjusting the reflectance properties locally. In contrast, we proposed a technique capable of producing surfaces with reflectance properties matching an arbitrary audience layout. Following the microfacet theory [22], we design our screens as a surface whose normal distribution approximates the desired reflectance. This manuscript is an extended version of our work [9]. It provides additional discussion and validation of light distributions provided by our designs, as well as an in-depth analysis of audience layouts for which our screens are suitable.

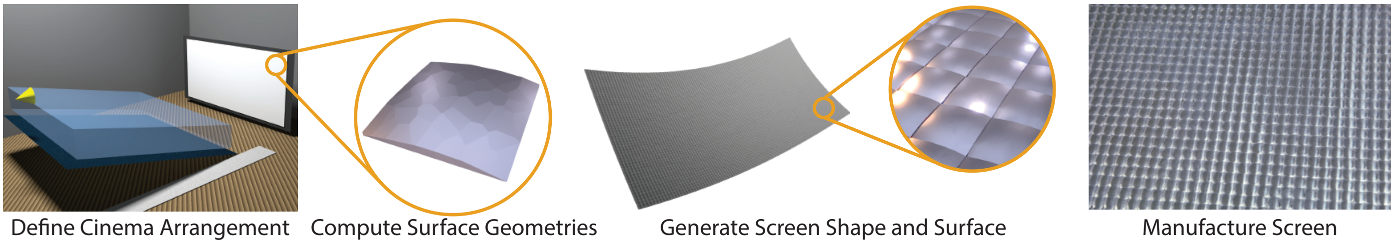

Fig. 2. Display generation overview: We start with the definition of the screen, the projector, and the audience. Based on this knowledge we uniformly sample the screen and for each position generate a microgeometry. These geometries are tiled and their heights adjusted to form the final screen surface. The screen surface is manufactured from aluminum on a CNC milling machine.

An alternative approach is to modify the direction of the light via microscopic optical diffusers [23, 24]. Recently, Crystal Screens [25] developed a new kind of reflective holographic screen with high gain (2.5) and a wide viewing angle (120°). However, the screen has limited size, up to 2.4×1.3 meters, and it is unclear how it can be used in cinemas where the average screen size is 16×7 meters.

Appearence Reproduction. Recent developments in computational fabrication enabled fabrication of objects with prescribed reflectance properties (i.e., BDRF and SVBRDF). To this end, several approaches have been proposed. Weyrich et al. [10] presented one of the first techniques to rely on a purely geometrical interpretation of BRDF, so-called microfacets theory [26, 27]. They proposed to build a surface from tiny, highly reflective "micro-mirrors" whose normal distribution matches the prescribed BRDF. The arrangement of these mirrors is computed using an expensive simulated annealing optimization. In contrast, our method is based on efficient convex optimization which allows us to compute much larger surfaces required for cinema screens. Rouiller et al. [28] has recently applied a similar idea. Instead of producing a surface with a desired facet arrangement, they proposed to compute tiny shapes – domes, which encode the BRDF properties. Later, they are placed on objects to affect their appearance. In contrast to the previous solution, this method does not produce a continuous surface. Recently, Levin et al. [29] considered the problem on a much smaller scale. Instead of using the geometrical interpretation of BRDF, they showed how to account for wave effects and change the appearance of the surface by controlling diffraction effects. They demonstrated impressive, high-resolution results with minimal feature size as small as 2-3 μm. However, due to high fabrication costs, they were able to demonstrate only small samples. Matusik et al. [30] proposed a different method for controlling and manufacturing material appearance. Instead of modifying local microgeometry, they suggested using inks with different reflectance properties, which when mixed, provide a broad range of spatially-varying BRDFs. Such an approach can also be combined with micro-facet techniques, where both geometry and inks are optimized to obtain the desired appearance [31, 32]. Instead of optimizing micro-geometry, it is possible to choose it from a precomputed database [33]. In contrast to these methods, we are the first to show how to efficiently generate spatially-varying BRDF for very large surfaces. Unlike many methods mentioned above, our technique is capable of producing exact reflectance properties under the assumption that the surface behaves as a mirror.

3. Display design

We take a geometrical approach for creating a screen surface and rely on the microfacet theory [34, 26, 35]. The overview of our technique is presented in Figure 2. To design the geometry of the screen surface, our method takes as an input the position and the size of the screen, projector location, and the audience. Without losing generality, we assume that the audience is defined as one or more polyhedrons which enclose the areas where viewers are expected. First, we consider a problem of computing small local shapes that for each location on the screen reflect light according to the audience description (Section 3.1). We formulate this problem by adopting a convex optimization for reconstruction of polyhedrons from Extended Gaussian Images [36]. In the next step, we combine local geometries into one surface (Section 3.2). Elevation of each shape is adjusted to minimize masking and shadowing. The non-uniform reflectance characteristic of our screen requires an additional content adjustment. We describe it in Section 3.3. We validate our designs in simulations and by manufacturing smaller screen sections from aluminum using a CNC milling machine (Section 5).

3.1. Microgeometry Design

The goal of the local geometry is to reflect incoming projector light only in directions where the audience is expected. Additionally, we should assure uniform luminance of the screen across different viewing directions. In other words, we want to create a microgeometry which acts as a diffuse surface, but only in the range of directions specified by the audience layout. In the regime of microfacet theory, producing such a surface is equivalent to designing a microgeometry composed of highly reflective facets whose normal distribution fulfills the requirement. We do this in two steps. First, we derive a set of facets defined by their normals and areas. Then we construct a convex, tileable shape from these facets.

Facet definition. In previous work, microfacet geometry was usually derived assuming that the size of every facet is equal. A set of microfacets was generated by sampling the desired normal distribution [10]. In our work, we propose to first derive facet normals and then adjust their areas to reproduce the desired BRDF. To this end, for a given location on the screen $\mathbf{x}$, we construct a set of directions $\mathbf{V_x}$ in which the projected light should be reflected. We uniformly sample all directions which lie in the half-space adjacent to the screen surface and include directions that intersect with the audience. For each direction $\mathbf{o}_i \in \mathbf{V_x}$ we define a corresponding normal vector of the facet $\mathbf{h}_i \in \mathbf{H_x}$ as $\mathbf{h}_i = (\mathbf{o}_i + \mathbf{i})/\|\mathbf{o}_i + \mathbf{i}\|$, where $\mathbf{i}$ is the direction of incident light – the direction towards the projector (Figure 3).

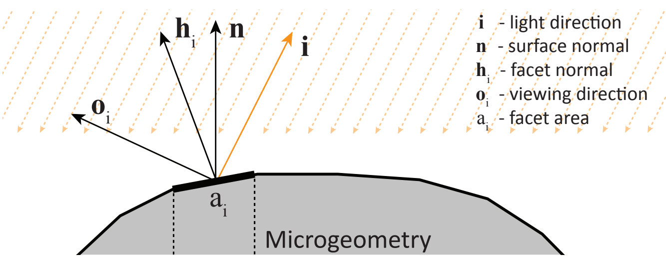

Fig. 3. Notation used in our derivation.

To complete the definition of the facets, we need to determine areas a_i for each of them, which will define the resulting BRDF. Walter et al. [37] presented an equation for specular microfacet-based BRDFs, where the reflectance of the surface is defined using a microfacet normal distribution function D:

$$\rho(\mathbf{i}, \mathbf{o}) = \frac{F(\mathbf{i}, \mathbf{h})\, G(\mathbf{i}, \mathbf{o}, \mathbf{h})\, D(\mathbf{h})}{4\, |\mathbf{i} \cdot \mathbf{n}|\, |\mathbf{o} \cdot \mathbf{n}|}. \tag{1}$$

Additional terms F and G denote Fresnel and masking-shadowing terms, respectively, and the operator $|\cdot|$ denotes the dot product between two vectors. For a comprehensive derivation, we refer the reader to [35]. In our case, we want to design a surface that has Lambertian reflectance in a range of directions corresponding to the audience viewing directions and does not reflect light outside. Therefore, we seek a microgeometry such that $\rho(\mathbf{i}, \mathbf{o}) = \rho$ for all $\mathbf{o} \in \mathbf{V_x}$, and $\rho(\mathbf{i}, \mathbf{o}) = 0$ for $\mathbf{o} \notin \mathbf{V_x}$. Note that $D(\mathbf{h})$ is in fact a normalized area of a facet with a normal $\mathbf{h}$; therefore, we can use Equation 1 to directly define the areas a_i as:

$$a_i = \frac{4\, \rho\, |\mathbf{i} \cdot \mathbf{n}|\, |\mathbf{o}_i \cdot \mathbf{n}|}{F(\mathbf{i}, \mathbf{h}_i)\, G(\mathbf{i}, \mathbf{o}_i, \mathbf{h}_i)}. \tag{2}$$

In our microsurface derivation, we can omit masking-shadowing term G as we construct convex shapes for which the term is constant. Furthermore, we assume that the light direction does not change for small microgeometries. Therefore, $|\mathbf{i} \cdot \mathbf{n}|$ is also constant. Because we are interested in reconstructing the microgeometry up to a scalar, all constant factors can be omitted and Equation 2 simplifies to:

$$a_i = \frac{|\mathbf{o}_i \cdot \mathbf{n}|}{F(\mathbf{i}, \mathbf{h}_i)}. \tag{3}$$

We wish to generate the geometry of small patches with the desired set of facet normals $\{\mathbf{h}_i\}$ and areas $\{a_i\}$. The patches also should tightly cover the screen surface. Consequently, we opted for patches with squared bases. As the desired sets of normals and areas that should form a microgeometry do not guarantee that the resulting shape will have a squared base, we add four additional faces. We call them side faces as they are perpendicular to the screen plane and form a rectangle on the screen surface. As we will demonstrate in this section, by optimizing the areas of the additional faces as well as their distances from the center of the microgeometry, it is possible to guarantee a perfect square-shape of the base. To summarize, we wish to generate microgeometries that have:

- faces with normals $\mathbf{H_x} = \{\mathbf{h}_i\}$ and corresponding areas $\mathbf{A_x} = \{a_i\}$,
- four side faces with normals $\pm\mathbf{r}, \pm\mathbf{s}$ and arbitrary but non-negative areas $a_{\mathbf{r}_{0,1}, \mathbf{s}_{0,1}}$, where the face normals are chosen orthogonal to each other and to the screen normal, i.e., $\mathbf{s} \cdot \mathbf{r} = 0, \mathbf{s} \times \mathbf{r} = \mathbf{n}$,
- no other faces with normals in the positive half-space of the screen surface.

We base our construction on Minkowski's theorem on convex polyhedra with prescribed normals and areas [38], which says that a polyhedron exists and is unique if the area-weighted face normals sum to zero. Given the constraints, this suggests requiring that the areas for side faces are identical, i.e., $a_{\mathbf{r}_0} = a_{\mathbf{r}_1}$ and $a_{\mathbf{s}_0} = a_{\mathbf{s}_1}$, and defining one additional face with area-weighted normal $-\sum_i a_i \mathbf{h}_i$ that serves as the base of our microgeometry.

Alexandrov [39] and Little [36] have found a variational principle for the problem when all areas are given. It is instructive to introduce their idea for solving the more general problem we have at hand here. Notice that the product of area and face normal $a_i \mathbf{h}_i$ is the gradient of the volume of a polyhedron relative to a face with normal $\mathbf{h}_i$ and area a_i. The fact these products sum to zero suggests that the polyhedron has extremal volume under variation of the distances l_i of the facets to the origin (i.e., a face i is contained in the plane $\mathbf{h}_i \cdot \mathbf{x} = l_i$). Alexandrov has found that the right constraint is to fix the sum of the area weighted distances $\sum_i a_i l_i = 1$ – with this constraint the polyhedron with maximal volume has the desired face areas. On the other hand Little suggests to fix the volume of the polyhedron and minimize $\sum_i a_i l_i$. Both formulations lead to an efficient convex optimization. In our implementation we decided to adapt the algorithm proposed by Little.

In our setting we also need to consider the side faces with areas $a_\mathbf{r}, a_\mathbf{s}$ (which are identical for opposing sides) and distances $l_{\mathbf{r}_{0,1}, \mathbf{s}_{0,1}}$. Let $\mathbf{l} = (l_0, \ldots)$ be the vector of distances. Together with the fixed facet normals $\{\mathbf{h}_i\}$, it defines the polyhedron, and therefore, its volume $V(\mathbf{l})$, as well as the areas of the facets $\{A_i(\mathbf{l})\}$. In addition to the volume being constant, we ask that the side faces intersect the base plane in a square and the free areas $a_\mathbf{r}, a_\mathbf{s}$ add up to a constant. More formally, we have the following constraints:

$$1 = V(\mathbf{l}), \quad l_{\mathbf{r}_0} + l_{\mathbf{r}_1} = l_{\mathbf{s}_0} + l_{\mathbf{s}_1}, \quad c = a_\mathbf{r} + a_\mathbf{s}, \tag{4}$$

where c is an additional constant fixed during the optimization. With these notations, the functional to be minimized is

$$\sum_i a_i l_i + a_\mathbf{r}(l_{\mathbf{r}_0} + l_{\mathbf{r}_1}) + a_\mathbf{s}(l_{\mathbf{s}_0} + l_{\mathbf{s}_1}). \tag{5}$$

Comparing this to the original formulation, we have added two free degrees of freedom, i.e., the area variables $a_{\mathbf{r}}, a_{\mathbf{s}}$, but also two new constraints (Equation 4). As a results, the degrees of freedom still match the number of constraints, and the solution is unique up to translation. We fix this last degree of freedom by setting the center of the polyhedron to be in the world's origin.

We iteratively minimize Equation 5 as a function of $\mathbf{l}$, under the constraints of Equation 4. As suggested by Little [36] each step is taken along the gradient of $\sum_i a_i l_i$ restricted to the hyperplane perpendicular to the gradient of the volume. This ensures that each step does not deviate significantly from the constraint $V(\mathbf{l}) = 1$. Note that we do also need to optimize for $l_{\mathbf{r}_{0,1}}, l_{\mathbf{s}_{0,1}}$. The reason is that $\mathbf{l}$ influences the areas $A(\mathbf{l})_{\mathbf{r}_{0,1}}, A(\mathbf{l})_{\mathbf{s}_{0,1}}$ of the side faces, which are supposed to be the same for opposite sides. So the variables $a_{\mathbf{r},\mathbf{s}}$ need to be adjusted, which we do by projecting the current values $A(\mathbf{l})_{\mathbf{r}_{0,1}}, A(\mathbf{l})_{\mathbf{s}_{0,1}}$ orthogonally onto the affine subspace:

$$0 = A(\mathbf{l})_{\mathbf{r}_0} - A(\mathbf{l})_{\mathbf{r}_1} \tag{6}$$
$$0 = A(\mathbf{l})_{\mathbf{s}_0} - A(\mathbf{l})_{\mathbf{s}_1} \tag{7}$$
$$2c = A(\mathbf{l})_{\mathbf{r}_0} + A(\mathbf{l})_{\mathbf{r}_1} + A(\mathbf{l})_{\mathbf{s}_0} + A(\mathbf{l})_{\mathbf{s}_1}. \tag{8}$$

The constraint on the distances to the side faces is similarly enforced by projecting onto the linear subspace given by the constraint $l_{\mathbf{r}_0} + l_{\mathbf{r}_1} - l_{\mathbf{s}_0} - l_{\mathbf{s}_1} = 0$. This formulation guarantees that the bounding box of each microgeometry is a square. The only criterion for generation of tileable geometries is that the side areas $a_{\mathbf{r}}, a_{\mathbf{s}}$ are sufficiently large, which can be enforced by appropriately choosing c. During our experiments we have found out that setting c proportionally to $\sum\{A_i(\mathbf{l})\}$ is sufficient for generating all examples described in the paper. The pseudocode of our method is described in Algorithm 1. Figure 4 shows snapshot of a microgeometry during optimization. At each iteration the geometry is tileable and the top faces change their area until they converge to the desired shape.

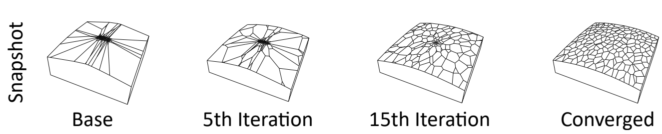

Fig. 4. Snapshots of example microgeometry during optimization.

Algorithm 1 Screen computation

$\mathbf{X} \leftarrow$ *positions of microgeometries*
$\{height_{\mathbf{x}}\} \leftarrow 0$ ▹ Setting the initial elevation to zero.
repeat ▹ Iterative computation of the elevation
  for all $\mathbf{x} \in \mathbf{X}$ **do**
    Sample the audience to determine $\mathbf{H_x}$
    Compute $\mathbf{A_x}$ according to $\mathbf{H_x}$ and Eq. 3
    Compute the normal of the microgeometry base $\mathbf{n_x}$
  end for
  Compute $\{height_{\mathbf{x}}\}$ by solving Poisson's equation for $\{\mathbf{n_x}\}$
until $\{height_{\mathbf{x}}\}$ does not change

for all $\mathbf{x} \in \mathbf{X}$ **do** ▹ Computation of individual microgeometries
  Set c proportionally to $\sum \mathbf{A_x}$
  Add two pairs of side facets to $\mathbf{H_x}$
  Add corresponding areas $a_{\mathbf{r}}$ and $a_{\mathbf{s}}$ to $\mathbf{A_x}$
  Set $\mathbf{l} = \{1\}$
  repeat ▹ Compute polyhedron for $\mathbf{H_x}$ and $\mathbf{A_x}$
    Reconstruct polyhedron from $\mathbf{H_x}$ and $\mathbf{l}$
    Scale $\mathbf{l}$ to satisfy $1 = V(\mathbf{l})$
    Update $\mathbf{l}$ as in [36]
    Adjust $a_{\mathbf{r},\mathbf{s}}$ to satisfy $c = a_{\mathbf{r}} + a_{\mathbf{s}}$
    Adjust $l_{\mathbf{r},\mathbf{s}_{0,1}}$ to satisfy $l_{\mathbf{r}_0} + l_{\mathbf{r}_1} = l_{\mathbf{s}_0} + l_{\mathbf{s}_1}$
  until Error of $\mathbf{A_x}$ is within tolerable threshold
end for

3.2. Screen Design

We demonstrated how to compute a microgeometry for an arbitrary location $\mathbf{x}$ on the screen surface. To build the entire screen, every location on its surface must be covered by microgeometry. This can be done by dividing the screen into a uniform grid. Then for each grid cell, a microgeometry can be computed according to our method (Algorithm 1). The microgeometries are generated up to scale. Therefore, we have to rescale each microgeometry before it is placed on the screen surface.

The screen surface computed using our optimization may have discontinuities between neighboring microgeometries, which can lead to masking and shadowing effects (Figure 5). To address this problem, we align the bases of microgeometries such that they form a smooth surface, minimizing the discontinuities. This is done by finding an appropriate elevation of each base by solving a discrete Poisson's equation, similarly to [10]. As we change the elevation, the location of each microgeometry with respect to the audience and the projector changes. Therefore, we have to interleave the solve of the Poisson's problem with updating the normals of the microgeometry bases. In practice, computation of the smooth screen surface requires several iterations of sequentially solving the Poisson's problem and updating the normals. The process is very fast as the reconstruction of individual microgeometries is not required at this stage.

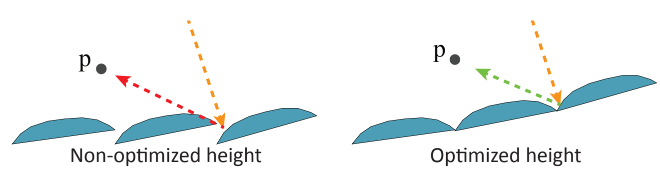

Fig. 5. When the screen surface has discontinuities, shadowing or masking can occur. In this case, a light ray coming from a projector (yellow) should be reflected towards position p. A discontinuous screen surface may shadow the reflected ray (left). This does not happen when the surface is continuous (right).

3.3. Content Preparation

Our screens are designed so that they reflect light uniformly, i.e., the brightness of any particular location on the screen does not depend on viewing direction. However, because the light reflected from the different parts of the screen spans different

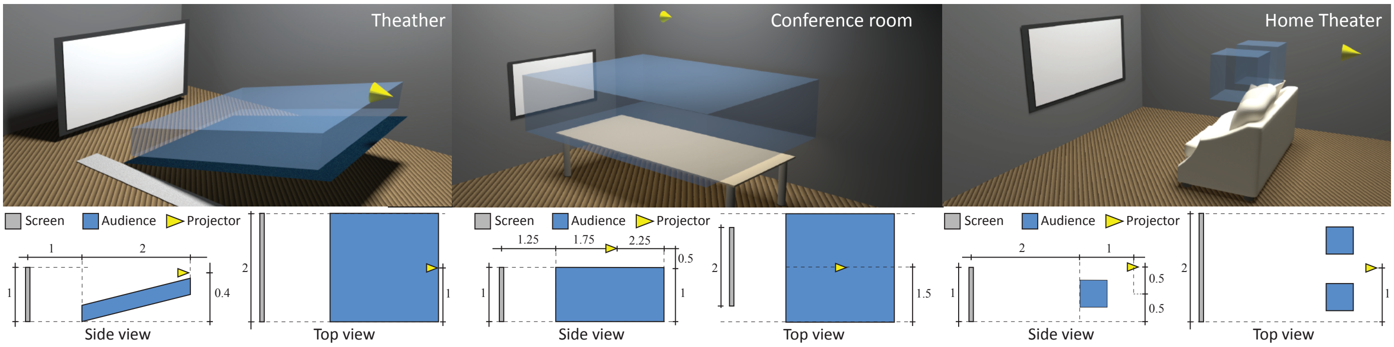

Fig. 6. We consider three installations in this paper. The first and the second setup depict one audience, in a theater and in a conference room. The third installation conceives a home theater with two separate audience spaces, for each viewer. Note that the units are left undefined as the design is general and can be scaled to different sizes. This also does not affect our screen computation.

solid angles, uniform illumination of the screen will not produce uniform brightness across the screen. The projector needs to be calibrated before an image is displayed. Intuitively, the areas of the screen which reflect the light in smaller angles should receive proportionally less light. The amount of light reflected in each direction should be proportional to the cosine of the viewing angle. Consequently, the total amount of light required at a given location $\mathbf{x}$ of the screen can be calculated as:

$$L(\mathbf{x}) = \int_{\Omega^+} cos\theta \cdot V(\Psi) \cdot d\omega_\Psi, \tag{9}$$

where function V has value 1 when the direction Ψ intersects with the audience volume and 0 otherwise. θ is the angle between the surface of the screen and Ψ. Depending on the definition of the audience, it might be difficult to compute L analytically. In our work, we computed it numerically. The most straightforward way of applying the compensation is to apply a darkening mask as a digital filter on the projector or as a filter inserted before the projector lens. This will not lead to the most efficient light use. However, we demonstrate that even with such a simple approach we can achieve a significant efficiency boost. More recently, new designs of HDR projector systems have been presented [7, 8]. Our screens are perfectly suitable for these solutions that can simply redirect the light illuminating each part of the screen according to Equation 9. In the next sections, we report results for both compensation methods.

4. Design Analysis

Our directional screens are composed of microgeometries which reflect light uniformly to the entire audience. Since individual microgeomtries are convex, a potential self-shadowing (masking) problem can occur only in the cavities of the screen, i.e., on a place where two different microgeometries are connected. Such self-shadowing can lead to light obstruction from certain geometries, self-reflections and consequently to uneven screen reflection. In this section, we will analyze the self-shadowing effect and its dependence on the position of the screen, the projector, and the audience. First, we will describe self-shadowing for the 2D case. Next, we will extend the analysis to arbitrary 3D designs. Finally, we will investigate example screen designs to check their feasibility. For a detailed derivation, please see the Appendix A.

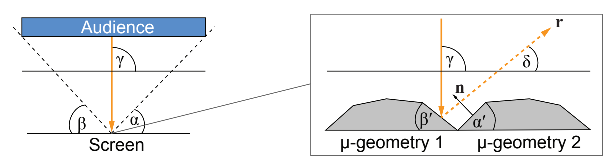

Fig. 7. Self-shadowing setup. At each location of the screen the ligh needs to be reflected to the audience parametrized by opening angles α and β. A light ray coming from direction γ is reflected from the microgeometry into direction δ. Self-shadowing occurs when the reflected angle δ is smaller than the angle of neighbouring microgeometry α'.

Self-Shadowing in 2D. The problem of self-shadowing is visualized in Figure 7. We have a light ray incoming at direction γ. The ray gets reflected from the microgeometry towards the audience in the direction $\mathbf{r}$. To avoid self-occlusions the reflected ray $\mathbf{r}$ should be at most parallel with the face of the neighboring microgeometry with the normal $\mathbf{n}$, i.e., $\angle(\mathbf{n}, \mathbf{r}) \leq 90$. We can make two important observations. The steeper the angle of the microgeometry, α', the more occlusion it will cause as it will be harder to satisfy the inequality. Similarly, the smaller the angle at which we reflect the light, δ, the higher the chance of self-occlusion. The smallest angle towards which we want to reflect the light from each microgeometry is towards the edges of the audience. At each location the audience can be parametrized by its extreme opening angles, expressed as α and β. Using this observation we can formulate the following inequality (detailed derivation in the Appendix A):

$$180 - \alpha - 2 \cdot \beta \leq \gamma \leq 2 \cdot \alpha + \beta. \tag{10}$$

This inequality is a necessary and sufficient condition for a screen free of self-shadowing. To determine the space of valid designs for a particular configuration of a screen and a projector we compute a range of incoming light directions γ. This and the Equation 10 allow us to specify a set of all opening angles α and β for which we can compute a valid directional screen. Applying the transitivity rule to Equation 10 leads to the following inequality:

$$\alpha + \beta \geq 60. \tag{11}$$

This inequality represents the theoretical limits of directional screens. Any screen with an audience span larger than 120 degrees will suffer from self-shadowing issues. The theoretical maximal opening angle can be achieved with rays incoming at exactly 90 degrees, i.e., parallel light projection, e.g., from a projector located at infinity.

Generalization to 3D. In the 3D case we have two arbitrary microgeometries composed of triangles. The cavity between neighboring geometries is represented as a common edge of two triangles from different microgeometries. Each triangle represents a reflection plane. This allows us to reformulate the problem: Given two intersecting planes, will a reflected ray be self-shadowed? Instead of applying general analysis, we can focus on the worst-case scenario. If a screen design is sound for the worst case it is guaranteed to avoid self-shadowing issues. First, let us take a closer look at the angle between the two planes. The smaller the opening angle, the higher the chance that a ray will be self-shadowed. Therefore, for our worst-case analysis we should take the smallest angle between the two planes. Next, we need to analyze the reflected rays. As an observation result from the 2D analysis, we can see that the wider the audience the higher the chance of self reflection. This means we should take the largest area visible from the cavity. Finally, we can apply the 2D analysis to see if the cavity will produce self-shadowing in the worst case.

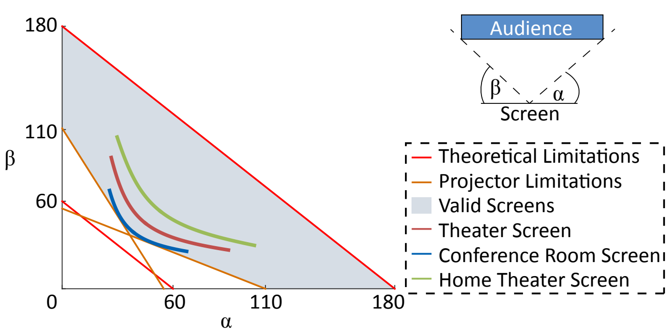

Fig. 8. Screen design space plot. Red straight lines mark theoretical limits of directional screens. Orange lines show the gamut of our particular screen-projector setup. Colored curves show our prototype screens. A directional screen reflects light from each point towards the entire audience. At a particular location we can parametrize this reflection by the opening angles α and β.

Feasibility of Prototype Screens. For our validation, we used three prototype designs (Figure 6). In each of the designs the screen center is located at world origins, and the screen is 2×1 meters. The projector is situated at the distance of 3 meters from the screen, which leads to incoming rays $\gamma \in [71.6°, 108.4°]$ (Figure 7). Figure 8 shows the space of valid designs of our directional screens. The limits indicated by red lines correspond to Equation 11 and show theoretical limits of our method. To compute the exact space of valid designs, we evaluate Equation 10 for the extreme values of γ, i.e., 71.6° and 108.4°. The resulting limits are visualized in orange, and we refer to them as screen-projector limitations. To summarize, the grey area in Figure 8 visualizes the set of values α and β which satisfy inequalities in Equations 10 and 11. Finally, for each prototype, we can iterate over all locations on the screen and compute the required pairs of α and β to visualize where our designs lie with respect to the constraints coming from the above analysis. These are visualized as curved lines in Figure 8. As it can be seen, all our designs are included into the valid space marked in grey. This means that there exists a valid solution for all the proposed designs, and by construction our algorithm is able to find these solutions. Please note that the dimensions in our analysis are relative and each setup can be scaled. Additionally, if the projector-screen setup is the same as in our analysis, the constrains on the valid design space remain the same. In case, the relative position of the projector or the screen size change, the Equations 10 and 11 have to be reevaluated.

5. Results

We evaluated our technique by both simulating (Section 5.2) several screen designs and fabricating (Section 5.3) their parts. Even though producing complex mirror surfaces is possible, we were limited by rather low-cost methods of fabricating our prototypes and chose to use a 3-axis CNC machine to mill our prototypes from aluminum. This allowed us to obtain highly glossy surfaces, but not perfect mirrors. On one hand, this worsens our results, but on the other hand, it validates the benefits of our design in cases when the fabrication is not perfect. We demonstrate in this section that even with such deviations from a perfect mirror-like BRDF we can achieve favorable results, i.e., brighter and more uniform screens, when compared to matte and high gain screens. Consequently, we also present simulation results obtained using the BRDF of polished aluminum. Despite the limitations of our low-cost manufacturing process, we argue that, in practice, surfaces that are much closer to mirrors can be achieved.

5.1. Technical Details

To validate our model we consider three screen designs. The first two are common use cases: a theater (Figure 6a) and a conference room (Figure 6b). To push our technique to the limits and demonstrate novel applications, we also present a home theater (Figure 6c) which creates a split view, i.e., the content can be observed only from two disjoint viewing volumes. Although such setups are not common, we believe they can find applications in custom visualization setups.

We generated the screens using microgeometries with 200 normals. This was determined based on the geometry size that we were able to simulate and manufacture. Since our screens are manufactured from polished aluminum, the Fresnel term is constant and the area of each microfacet was solely determined by the viewing angle. To optimize the trade-off between geometry precision and the computational time, we terminated the optimization when there was no facet whose area deviated by more than 1% from the desired value. The size of the microgeometries plays an important role. The images produced by our screen are composed of tiny reflections spaced by the distance equal to the size of one microgeometry. Therefore, the size of the microgeometry should be small enough to make individual reflections invisible for a human eye but also big enough to enable fabrication and to avoid diffraction effects. In our simulations and physical prototypes, we used microgeometries with a width of 4 mm which corresponds to 4K (4096×2160) resolution of an average cinema. These numbers for geometry spacing are also consistent with LED screen manufacturers [40]. Note that the images produced with our screens are similar to those produced by big LED video walls where the size of LEDs is significantly smaller than the spacing between them.

All computations were run on Intel Xeon Processor E5-1620 v3. A total of 125k microgeometries were computed for each screen. An average microgeometry was computed in approximately 2 seconds, and the computation of the whole screen took roughly 6 hours. We analyzed the convergence of our square microgeometry computation algorithm. We randomly sampled geometries across all three of our designs and plotted their convergence (Figure 9). Since we base our algorithm on convex optimization proposed by [36], the most computationally demanding step at each iteration is the reconstruction of the connectivity of the geometry. This is computed using a convex hull algorithm running in $O(n \log n)$. An average geometry converges in approximately 50 iterations.

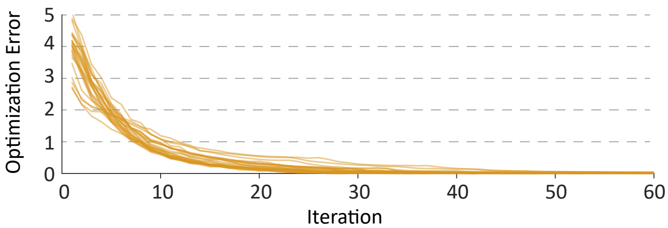

Fig. 9. Convergence plot of randomly selected microgeometries.

5.2. Simulations

To simulate our screens, we used a physically-correct ray tracer that accounts for both shadowing and masking. For each screen, we created a virtual testing room by placing a screen, a projector, and an audience at their respective positions. Screens are modeled with a BRDF corresponding to polished aluminum. For each screen, we calculate the corresponding calibration mask (Figure 10) and model it as a modulation layer of the projector. In our simulation, we also accounted for human visual acuity. We assumed that the individual reflections from neighboring microgeometries are not resolved by the human visual system. To account for this, we filtered all our renderings using a Gaussian filter with a standard deviation corresponding to a visual angle spanned by one microgeometry seen from the middle of the audience. This is a realistic assumption for the movie theater case. Given a medium screen size (15 m) and the often mentioned optimal viewing angle of 36° (THX), the resulting viewing distance is roughly 23 m. The visual angle spanning one microgeometry used in our experiments (4 mm) is equal to 0.6 arcmin, which is below the smallest gap that an observer with 20/20 vision can perceive. We evaluated the screens regarding their efficiency, as well as brightness uniformity across the screen and the audience. Finally, we simulated images shown on our screens. For full simulations, please refer to the supplemental video.

Fig. 10. Calibration masks used to equalize the brightness across each screen.

First, we evaluated the distribution of the brightness provided by our screen across the audience by rendering illuminated screens from uniformly sampled locations within the audience. Since the split screen is symmetrical, we show results for the left view only. To limit aliasing problems, the views were computed in resolution 5×FullHD so that each microgeometry occupies more than one pixel. Next, we computed the average brightness for each view and plotted it as a function of position in the audience (Figure 11). As expected, due to the BRDF used in our experiment that slightly deviates from a perfect mirror reflection, the brightness provided by our directional screen is not perfectly uniform. The variation is, however, very small for the theater and conference room cases. The effect is more pronounced for the home theater. We attribute this to the relatively small audience size compared to the screen.

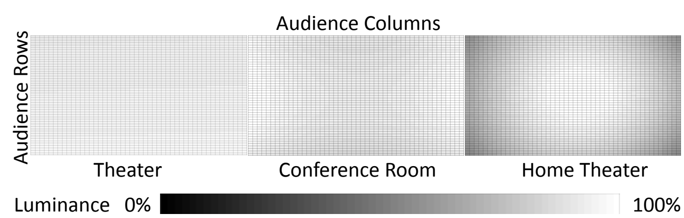

Fig. 11. Screen brightness as a function of location within the audience.

Next, we evaluated the uniformness of brightness in a single view. To this end for each screen, we sampled three random locations in the audience, shown in Figure 12, and rendered the corresponding views. We expressed the resulting brightness as the percentage deviation from the mean brightness of the screen and visualized the brightness variation in each view using histograms (Figure 12). Ideally, the histograms should form a peak around mean brightness (zero value in our histograms), which would mean a perfectly uniform distribution of the light. We compared our directional screens with the high gain screen, shown as black lines in Figure 12. We can see that our directional screens achieved higher peaks in histograms which also span smaller ranges of values. There are several factors that led to imperfect histograms for our solution: rendering aliasing, assumed BRDF, the limited number of facets. However, even with these limitations we achieved better brightness distribution than currently used high-gain screens.

Then, we compared our designs in terms of efficiency and brightness uniformity with matte and high gain screens. We did this by rendering a white patch on each screen according to ISO 3640-1976 [41]. Figure 13 shows gain provided by each

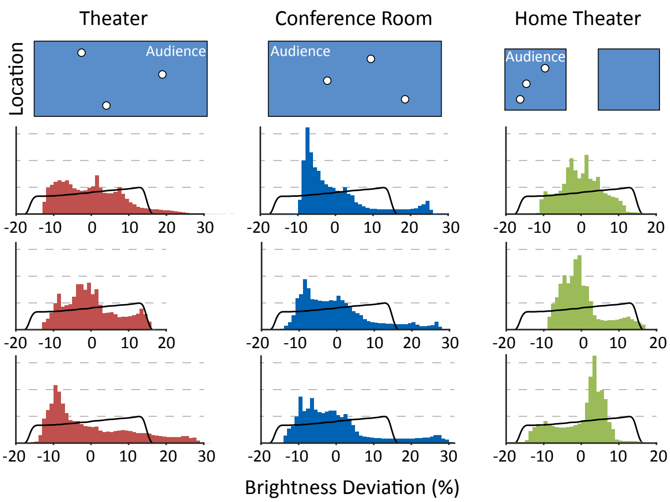

Fig. 12. We randomly sampled viewing locations in the audience (white dots). For each location a corresponding histogram shows distribution of relative brightness with respect to the mean. We compared it with a high-gain screen, shown as a black line.

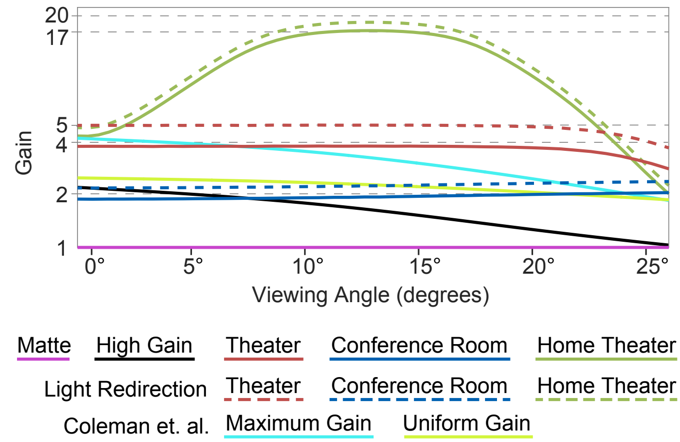

Fig. 13. Brightness (gain) of each screen relative to the brightness provided by a matte screen. Gain is presented on a logarithmic scale which better corresponds to human perception. Solid lines represent our screens with calibration performed by light attenuation, dashed lines with a projector which redirects light [8].

screen relative to a matte screen as a function of viewing angle. The results demonstrate that even with a glossy BRDF our screens provided better and more uniform brightness. We also compared our directional screens to designs proposed by Coleman et al. [21]. The patent presents two designs optimizing for maximum gain or uniformness of reflection (Figure 13 cyan and lime, respectively). When maximizing the gain, the design exhibits characteristics similar to high-gain screens where the glossy lobe decays after a small peak. On the other hand, the uniform design achieves significantly lower gain. Contrary to this our directional screens combine the advantages of both screens and provide high-gain and uniform reflection (Figure 13 red). In our experiments, we performed projector calibration by light attenuation. Using newer projector designs with light redirection [8], we can achieve 20% higher for each screen (dashed lines in Figure 13). The improvement in brightness is related to the audience size. The larger the audience, the lower the average gain of a directional screen.

Finally, in Figure 19, we present a comparison of images displayed on directional and matte screens. To generate these results we project an image onto the screen and capture its reflections at three points in the audience: the left corner, center, and the right corner of the middle row. We can see that our directional screens are significantly brighter. Moreover, the image brightness is consistent across the whole audience. Please note that the middle image for the home theater screen is from a viewing location outside the considered audience. Therefore, the non-uniform brightness of the directional screen at this view is expected.

5.3. *Fabricated Prototypes*

In addition to our simulations, we also fabricated central fragments of our designs. Different techniques can be used to manufacture such surfaces, e.g., milling, 3D printing, embossing, etc. We chose milling as it offers high fabrication accuracy and a wide range of materials, including highly reflective ones such as aluminum. Due to the time requirements for milling the geometry on a non-professional device as well as the relatively small working volume of our machine, we were able to fabricate only small fragments of our theater and home cinema screens.

Milling the Geometry. We used a 3-axis milling machine, Roland EGX-600 with a 10 micron step resolution, for manufacturing of the prototypes (Figure 15). We chose hard aluminum, which was manually polished after milling to achieve mirror-like reflectance. Reproduction of small cavities in the final screen was challenging due to technical limitations (i.e., step and tool size) and some cavities could not be perfectly reproduced. For the validation we milled two prototypes (Figure 15). The first prototype has a size of 20×20 cm and corresponds to the theater directional screen. The second prototype has a size of 10.5×7 cm and mimics the home theater split audience setup.

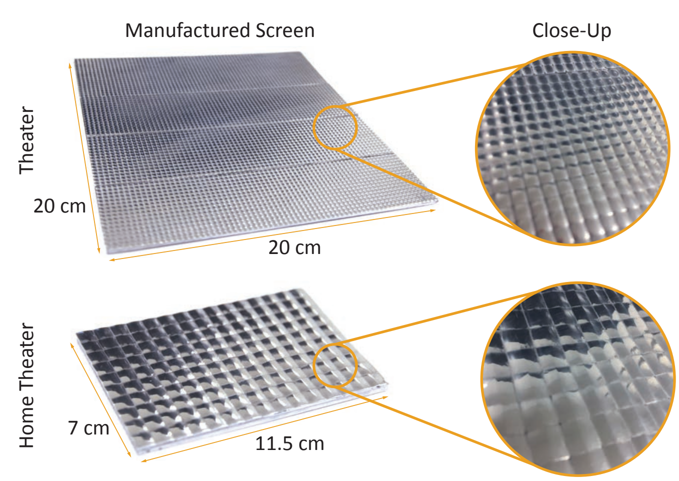

Fig. 15. Photos of manufactured prototypes of a uniform and a split directional screen.

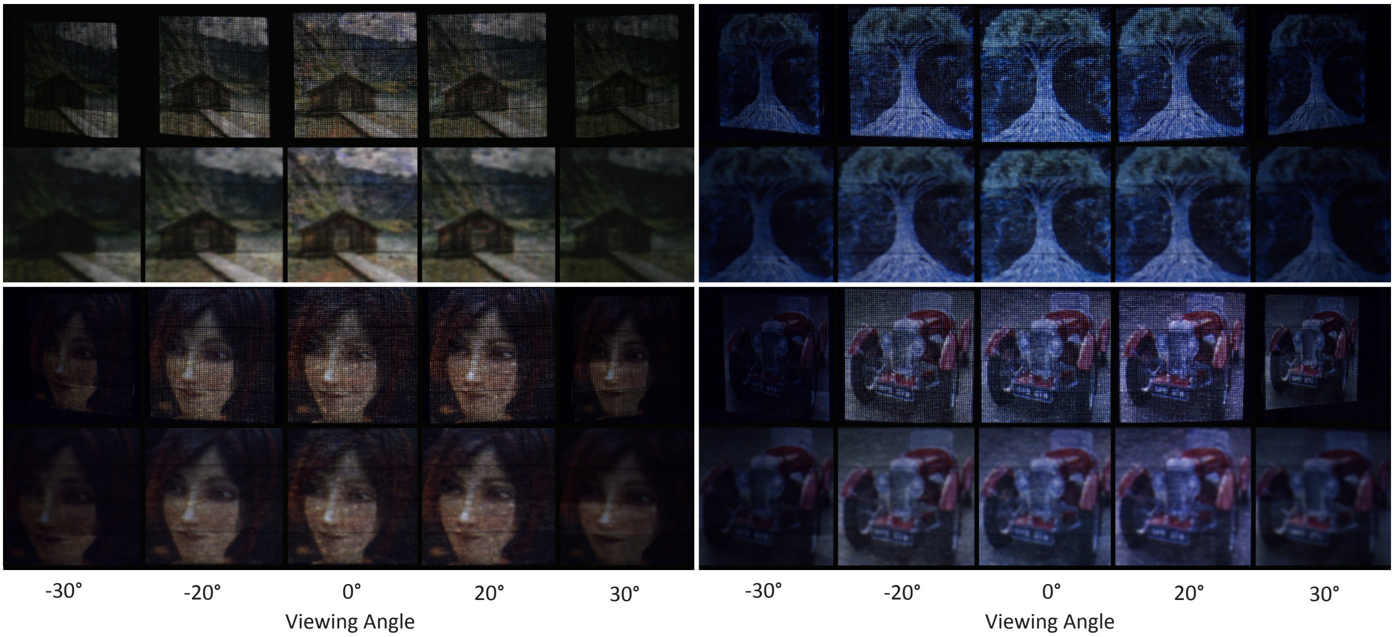

Fig. 14. Manufactured prototype reflecting four images, viewed from various directions, captured by camera setup B. According to the display specification, the reflection should be visible between 0 and 20 degrees (three middle columns). Outside this range (the first and the last column), the image should be dark. The top row of each pair shows raw captures, and the bottom row shows images after applying Gaussian filtering simulating the point spread function of the human eye.

Capturing Setup. We have validated the fabricated prototypes by recreating our design setups. Two validation setups were used to evaluate screen reflection and audience coverage (Figure 16). To evaluate the audience coverage of a directional screen, we captured the shape of its reflection on a matte screen (Camera A), which should approximate the audience as closely as possible. The second setup evaluated the images provided to the viewers at different locations in the audience. To this end, we emulated a viewer moving through the audience while looking at the screen (Camera B). The photos were captured using a Nikon D750 camera. We used the following exposure settings to prevent overexposed regions in captured images: ISO 100, shutter speed 1/30s and aperture F14.

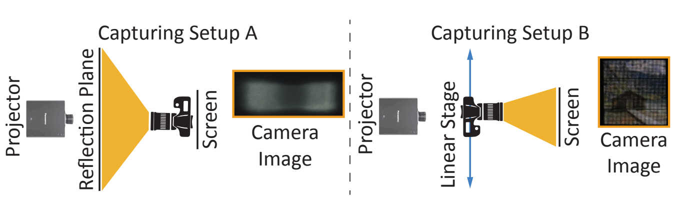

Fig. 16. Prototype capture setup. A camera captures the audience coverage of the examined directional screen (A). A second camera on a linear stage captures the reflection from the directional screen (B).

Prototype Photo Results. Figure 17 shows results of the audience coverage test. We show, side by side, a simulation of the reflection and the actual reflection captured with our camera setup A. We can see that our prototypes match the specified shape while providing light to the entire audience. A fraction of the reflected light bleeds outside the audience. We attribute this behavior to the BRDF of polished aluminum used in our simulations as well as manual polishing which may affect the accuracy of our geometries. For the home theater, there is also a reflection visible between the two audience volumes. This is caused by polishing, which removes sharp edges necessary for reproduction of perfect split audiences.

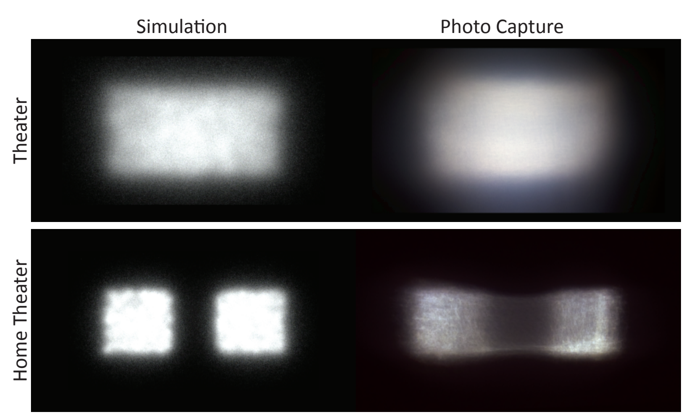

Fig. 17. A directional screen reflection towards the audience. Simulations (left) are compared with fabricated prototypes (right).

We also evaluated the images produced by our screens as seen by viewers. To this end, using camera setup B we captured the illuminated screens from several viewing locations (Figure 14). The top row of each pairs shows the capture from the camera. The alignment of screen pixels with the camera causes the impression of individually lit points. However, to the human, the screen looks uniform due to the point spread function of the eye. We approximate the effect by applying Gaussian filtering (Section 5.2). Our fabricated screen provides the highest brightness in the desired range (0-20 degrees), and becomes dim outside of this range.

Light Efficiency. To demonstrate the difference between our directional screen and the current state-of-the-art screen designs, we compared our screen with commercially available alternatives: diffuse matte screens, and silver high gain cinema screens. The matte screen reflects incoming light uniformly, imitating a Lambertian surface. For silver screens, we used a Ballantyne Strong Premium HGA 2.9 Silver Screen [42]. This type of screen offers higher brightness but only within a limited angular range which is required to cover the audience. We measured reflected luminance from each screen within ±30° using MINOLTA LS-100 Luminance Meter according to ISO 3640-1976 [41]. The measurements are compared in Figure 18.

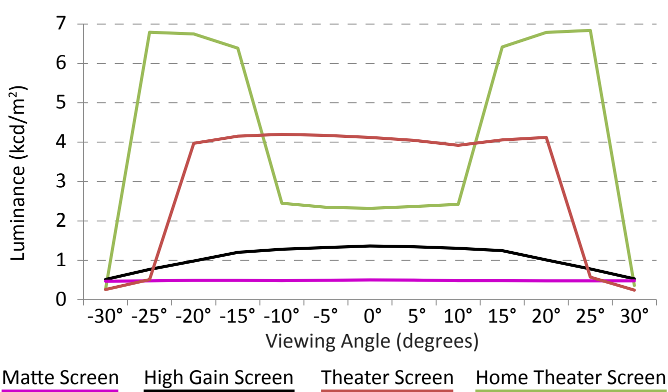

Fig. 18. Luminance measurements of home cinema directional screen (green), theater directional screen (red), cinema silver screen (black), and matte screen (purple) across 60 degrees of viewing angle.

The matte screen showed an almost constant brightness from all viewing angles. The silver screen shows a non-constant behavior with the strongest reflection in the normal direction. The brightness decreases with a growing viewing angle. In contrast, our directional screen maintains uniform brightness over the whole audience area. For our theater screen, the overall light efficiency is more than eight times higher when compared to the matte screen and almost three times higher than the brightest spot of the silver screen. The directional screen generated for the home cinema setup reaches even higher brightness values.

6. Discussion and Limitations

Brightness Gain. The brightness gain of directional screens depends on the audience size. From our design analysis, we know that the audience size is limited and cannot be arbitrary. This will always manifest as an increase in brightness when compared to a matte screen. The advantage when compared to a high-gain screen is uniformness of the reflected light. For large audience sizes, a high-gain screen might achieve higher peak brightness. However, this peak will quickly diminish as one moves away from the center of the audience. A directional screen is capable of providing a uniform brightness across the whole audience.

Fabrication Limitations. Due to the limitations of manufacturing software, we were forced to use a relatively small amount of microgemetries (200) per pixel of the screen. As a result, our generated geometries have sharp angles and discontinuities. Combined with the glossy BRDF of polished aluminum these discontinuities manifest as sharp specular reflections. This makes a large discrepancy between the image of a directional screen captured by a camera and the one seen by human observers. The camera sees each microgeometry as an individual bright spot akin to taking a picture of an LED screen (Figure 14). We approximate how a directional screen would look like when viewed by a human observer by applying Gaussian filtering with a small kernel. However, this is merely an approximation of the human visual system and introduces a speckle artifact. Specialized methods taking into account human perception need to be used to faithfully capture a screen consisting of individual bright reflections [43] and could be an interesting direction for future work.

Using our low-cost manufacturing technique, a perfect reproduction of our designs was challenging. Our milling machine could not reproduce small cavities. Also, the manual polishing affected the accuracy of the geometry. This is manifested as an uneven brightness of the physical prototypes (Figure 14) which was not present in our simulated results (Figure 19). Our surfaces also have a small diffuse component. This compensates for a limited number of microgeometry facets but also causes some light bleeding on the boundaries of the audience.

Our fabrication technique is not ideal for large-scale mass production. We believe that embossing and coating the surface with aluminum pigments, similarly to [44], can be used for commercial purposes. Since cinema chains provide standardized rooms, e.g., a standard IMAX screen is 22 × 16.1 m, and the audience remains similar across different venues, it is possible to split the screen into tiles and fabricate reusable embossing forms. Since our screen can be viewed as a surface with smoothly varying reflectance properties, small misalignments between the tiles as well as between the screen and the projector should not cause visible problems.

Due to our fabrication limitations and limited details in the literature about other designs, the comparison to commercial solutions, such as Crystal Screens [25] and the design proposed by Coleman et al. [44], is challenging. We provide only gain curves comparison which demonstrates the benefits in terms of the brightness for high-gain screens and [44]. Additional analysis is necessary to include other screens and account for the overall image quality, e.g., color, and contrast reproduction. In the future, it also is essential to examine cost-quality trade-offs to identify the best solutions for cinema projection screen. This aspect was omitted in this work.

In our work, we opted for square tiling because of its natural mapping to projector pixels. Other tilings may lead to surfaces that are easier to fabricate. However, we believe the optimal tile shape depends on the reflectance of each location on the screen. Therefore, in the future, it would be interesting to consider tiling of shapes that vary across the surface of the screen.

7. Conclusion

We presented an algorithm for generating directional projection screens. It improves over currently used high gain screens in two areas. First, our screens can achieve higher gain factors. Second, our design can eliminate the hot-spot effect which affects traditional high gain screens. These improvements can provide a better viewing experience and substantial energy savings for theaters. Furthermore, we provided analysis of feasible audience layouts. From this analysis, we derived theoretical, setup-specific limits of directional screens. Using these limits as guidelines, one can generate occlusion-free screen designs. Besides the theoretical model, we also provided a validation using realistic simulation and fabrication techniques. We used polished aluminum which is cost-effective and relatively easy to tool. Even though there are several limitations regarding our fabrication process, we demonstrated that our prototypes are more uniform and achieve higher brightness than current high gain screens. We believe that using more advanced manufacturing techniques can further improve the results and match the theoretical capabilities of our technique.

References

[1] Cowan, M. REALD 3D theatrical system. A technical overview. In: European Digital Cinema Forum. 2008,.
[2] Lit, A. Depth-discrimination thresholds as a function of binocular differences of retinal illuminance at scotopic and photopic levels. JOSA 1959;49(8):746–751.
[3] Bartleson, C, Breneman, E. Brightness perception in complex fields. JOSA 1967;57(7):953–957.
[4] Shin, JC, Yaguchi, H, Shioiri, S. Change of color appearance in photopic, mesopic and scotopic vision. Optical review 2004;11(4):265–271.
[5] Schuck, M, Sharp, G. 3D digital cinema technologies. Journal of the Society for Information Display 2012;20(12):669–679.
[6] Harkness Screens. `http://www.harkness-screens.com/2d-3d-overview.html`; 2014.
[7] Hoskinson, R, Stoeber, B, Heidrich, W, Fels, S. Light reallocation for high contrast projection using an analog micromirror array. ACM Trans Graph 2010;29(6):165:1–165:10.
[8] Damberg, G, Gregson, J, Heidrich, W. High brightness HDR projection using dynamic freeform lensing. ACM Trans Graph 2016;35(3):24:1–24:11.
[9] Piovarči, M, Wessely, M, Jagielski, M, Alexa, M, Matusik, W, Didyk, P. Directional screens. In: Proceedings of the 1st Annual ACM Symposium on Computational Fabrication. ACM; 2017, p. 1:1–1:10.
[10] Weyrich, T, Peers, P, Matusik, W, Rusinkiewicz, S. Fabricating microgeometry for custom surface reflectance. ACM Trans Graph 2009;28(3):32:1–32:6.
[11] Tompkin, J, Heinzle, S, Kautz, J, Matusik, W. Content-adaptive lenticular prints. ACM Trans Graph 2013;32(4):133.
[12] Damberg, G, Heidrich, W. Efficient freeform lens optimization for computational caustic displays. Optics express 2015;23(8):10224–10232.
[13] Patow, G, Pueyo, X. A survey of inverse surface design from light transport behavior specification. In: Computer Graphics Forum. 2005, p. 773–789.
[14] Chandler, J, De Palma, J. High-brightness projection screens with high ambient light rejection. Journal of the SMPTE 1968;77(10):1012–1024.
[15] Richards, M, Schnuelle, D. The effective gain of a projection screen in an auditorium. SMPTE Motion Imaging Journal 2010;119(7):62–67.
[16] Berggren, G, Carignan, D. On optimizing screen curvature in a front-projection indoor theater. Journal of the SMPTE 1967;76(11):1104–1106.
[17] Cobb, S, Conder, TM, Vanderwerf, DF. Directional front projection screen. 1980. US Patent 4,206,969.
[18] Van De Ven, JC. Front projection screen. 1990. US Patent 4,911,529.
[19] Hockley, BS, Pawluczyk, R. Chromatically corrected directional diffusing screen. 1991. US Patent 5,046,793.
[20] Sun, B. Front ptojection screen. 2001. WO Patent 2,001,033,298.
[21] Coleman, DA, Sharp, GD. Polarization preserving front projection screen microstructures. 2011. US Patent App. 13/290,978.
[22] Ashikmin, M, Premože, S, Shirley, P. A microfacet-based BRDF generator. In: Proceedings of the 27th annual conference on Computer graphics and interactive techniques. 2000, p. 65–74.
[23] RPC Photonics. `https://www.rpcphotonics.com/`; 1980. Accessed: 2016-04-08.
[24] Luminit. `https://www.luminitco.com/`; 2016.
[25] Crystal Screens. `http://www.crystalscreens.com/`; 2016.
[26] Cook, RL, Torrance, KE. A reflectance model for computer graphics. ACM Trans Graph 1982;:7–24.
[27] Blinn, JF. Models of light reflection for computer synthesized pictures. In: ACM SIGGRAPH Computer Graphics. 1977, p. 192–198.
[28] Rouiller, O, Bickel, B, Matusik, W, Alexa, M, Kautz, J. 3D printing spatially varying BRDFs. IEEE Computer Graphics and Applications 2013;33:48–57.
[29] Levin, A, Glasner, D, Xiong, Y, Durand, F, Freeman, W, Matusik, W, et al. Fabricating BRDFs at high spatial resolution using wave optics. ACM Trans Graph 2013;32(4):144:1–144:14.
[30] Matusik, W, Ajdin, B, Gu, J, Lawrence, J, Lensch, HPA, Pellacini, F, et al. Printing spatially-varying reflectance. ACM Trans Graph 2009;28(5):128:1–128:9.
[31] Malzbender, T, Samadani, R, Scher, S, Crume, A, Dunn, D, Davis, J. Printing reflectance functions. ACM Trans Graph 2012;31(3):20:1–20:11.
[32] Lan, Y, Dong, Y, Pellacini, F, Tong, X. Bi-scale appearance fabrication. ACM Trans Graph 2013;32(4):145:1–145:12.
[33] Wu, H, Dorsey, J, Rushmeier, H. Inverse bi-scale material design. ACM Trans Graph 2013;32:163:1–163:10.
[34] Torrance, KE, Sparrow, EM. Theory for off-specular reflection from roughened surfaces. JOSA 1967;57(9):1105–1112.
[35] Heitz, E. Understanding the masking-shadowing function in microfacet-based BRDFs. Journal of Computer Graphics Techniques 2014;3(2).
[36] Little, JJ. An iterative method for reconstructing convex polyhedra from Extended Gaussian Images. In: Proc. of AAAI-83. Washington, DC; 1983, p. 247–250.
[37] Walter, B, Marschner, SR, Li, H, Torrance, KE. Microfacet models for refraction through rough surfaces. In: Proceedings of the 18th Eurographics Conference on Rendering Techniques. Eurographics Association; 2007, p. 195–206.
[38] Minkowski, H. Ausgewählte arbeiten zur zahlentheorie und zur geometrie: Mit D. Hilberts Gedächtnisrede auf H. Minkowski, Göttingen 1909; chap. Allgemeine Lehrsätze über die konvexen Polyeder. Vienna: Springer Vienna; 1989, p. 121–139.
[39] Alexandrov, AD. Convex Polyhedra. Springer; 2005.
[40] Christie Digital Systems USA, I. LED display walls (whitepaper). Tech. Rep.; Christie Digital Systems USA, Inc; 2016.
[41] ISO 3640-1976. Cinematography. television usage. specification for motion-picture prints and sound records for international exchange of television programmes. Standard; International Organization for Standardization; Geneva, CH; 1978.
[42] Ballantyne Strong Inc. `http://screen.ballantynestrong.com`; 2015.
[43] Radiant Imaging, I. Making LED screens look great! methods for LED video screen correction. Tech. Rep.; Radiant Imaging, Inc.; 2009.
[44] Coleman, DA, Sharp, GD. 54.2: Invited paper: high efficiency polarization preserving cinema projection screens. In: SID Symposium Digest of Technical Papers. 2013, p. 748–751.

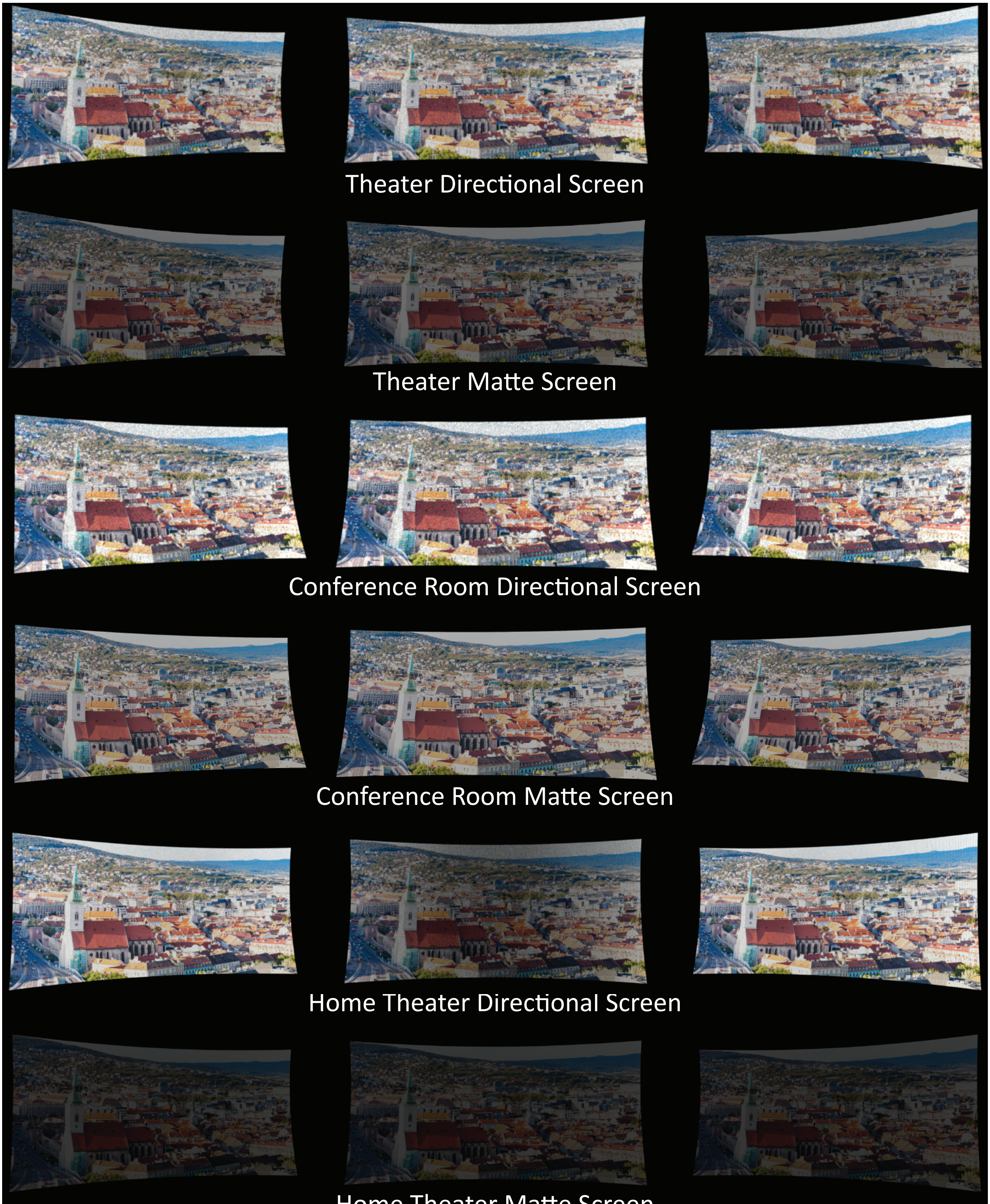

Fig. 19. Renderings of an image projected on a directional screen and a matte screen. Please note that the middle image for the home theater screen is from a viewing location outside the considered audience. Therefore, the non-uniform brightness for the directional screen can be observed for this view.

Appendix A. Directional Screen Limits Derivation

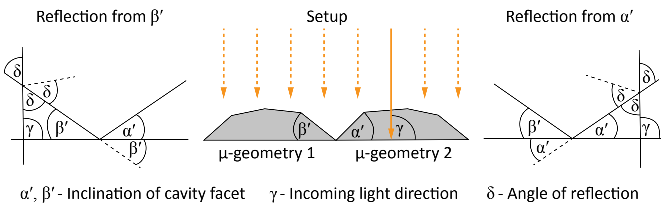

Fig. A.20. Self-shadowing parametrized with facet angle.

To analyze self-shadowing we start by parameterizing each cavity (Figure A.20 middle). We parametrize the cavity facets by their opening angles α' and β'. The incoming light ray is parametrized by its direction γ. When the ray hits one of the facets it is reflected under an angle δ. This gives rise to the first inequality:

$$\alpha' + \beta' \leq \delta, \tag{A.1}$$

which tells us that δ should be always bigger than the sum of cavity facet opening angles. To further analyze Equation A.1 we split this into two cases. Case one is when the incoming ray hits facet α' (Figure A.20 right):

$$\begin{aligned} &\delta = \gamma - \alpha', \\ &\alpha' + \beta' \leq \gamma - \alpha', \\ &\gamma - 2 \cdot \alpha' - \beta' \geq 0, \end{aligned} \tag{A.2}$$

and case two is when incoming light hits facet β' (Figure A.20 left):

$$\begin{aligned} &\delta = 180 - \gamma - \beta', \\ &\alpha' + \beta' \leq 180 - \gamma - \beta', \\ &\gamma + \alpha' + 2 \cdot \beta' \leq 180. \end{aligned} \tag{A.3}$$

However, this parametrization is impractical. In order to use it to check the validity of a setup, we would need to check every location of the screen and compute all possible cavity facets. Therefore, we reparametrize the problem to use the opening angles of the audience visible from a particular location.

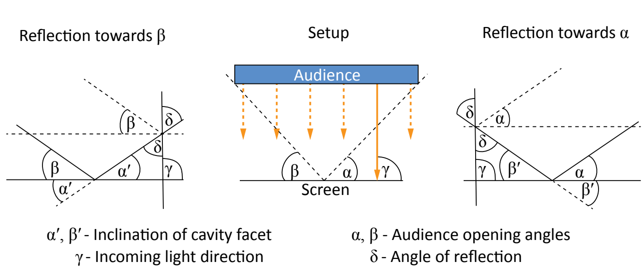

Fig. A.21. Reparameterization using the opening angle of the audience.

Each position is parametrized using the opening angles of the audience (Figure A.21 middle). The light should be reflected uniformly towards the entire audience. Each direction corresponds to a unique inclination of cavity facets. We can observe that there is an inverse relationship. The smaller the angle towards which we reflect the light, the bigger the angle of the corresponding microfacet. In other words, the wider our audience is, the sharper cavities will be generated, inevitably leading to self-occlusions. Therefore, in order to analyze the worst case we should look at the widest part of the audience. Using the opening angles we can express corresponding facets reflecting light towards the edges of the audience. First we consider reflection towards β (Figure A.21 left):

$$\begin{aligned} \alpha' &= \gamma - \delta, \\ \delta &= \beta + \alpha', \\ \alpha' &= \gamma - \beta - \alpha', \\ \alpha' &= \frac{\gamma - \beta}{2}, \end{aligned} \tag{A.4}$$

and similarly reflection towards α (Figure A.21 right):

$$\begin{aligned} \beta' &= 180 - \gamma - \delta, \\ \delta &= \alpha + \beta', \\ \beta' &= 180 - \gamma - \alpha - \beta', \\ \beta' &= \frac{180 - \gamma - \alpha}{2}. \end{aligned} \tag{A.5}$$

Plugging Equations A.4 and A.5 into Equations A.2 and A.3 gives:

$$\begin{aligned} &\gamma - 2 \cdot \alpha' - \beta' \geq 0, \\ &\gamma + \alpha' + 2 \cdot \beta' \leq 180, \end{aligned}$$

$$\begin{aligned} &\gamma - 2 \cdot \frac{\gamma - \beta}{2} - \frac{180 - \gamma - \alpha}{2} \geq 0, \\ &\gamma + \frac{\gamma - \beta}{2} + 2 \cdot \frac{180 - \gamma - \alpha}{2} \leq 180, \end{aligned}$$

$$\gamma + \alpha + 2 \cdot \beta \geq 180, \tag{A.6}$$

$$\gamma - 2 \cdot \alpha - \beta \leq 0. \tag{A.7}$$

Finally, combining Equations A.6 and A.7, we get the limits of directional screens.

$$180 - \alpha - 2 \cdot \beta \leq \gamma \leq 2 \cdot \alpha + \beta. \tag{A.8}$$